Comparison and critical analysis of invariant-based models with respect to their ability in fitting human aortic valve data

F. Auricchio, A. Ferrara & S. Morganti

Annals of Solid and Structural Mechanics

ISSN 1867-6936

Ann. Solid Struct. Mech.
DOI 10.1007/s12356-012-0028-x

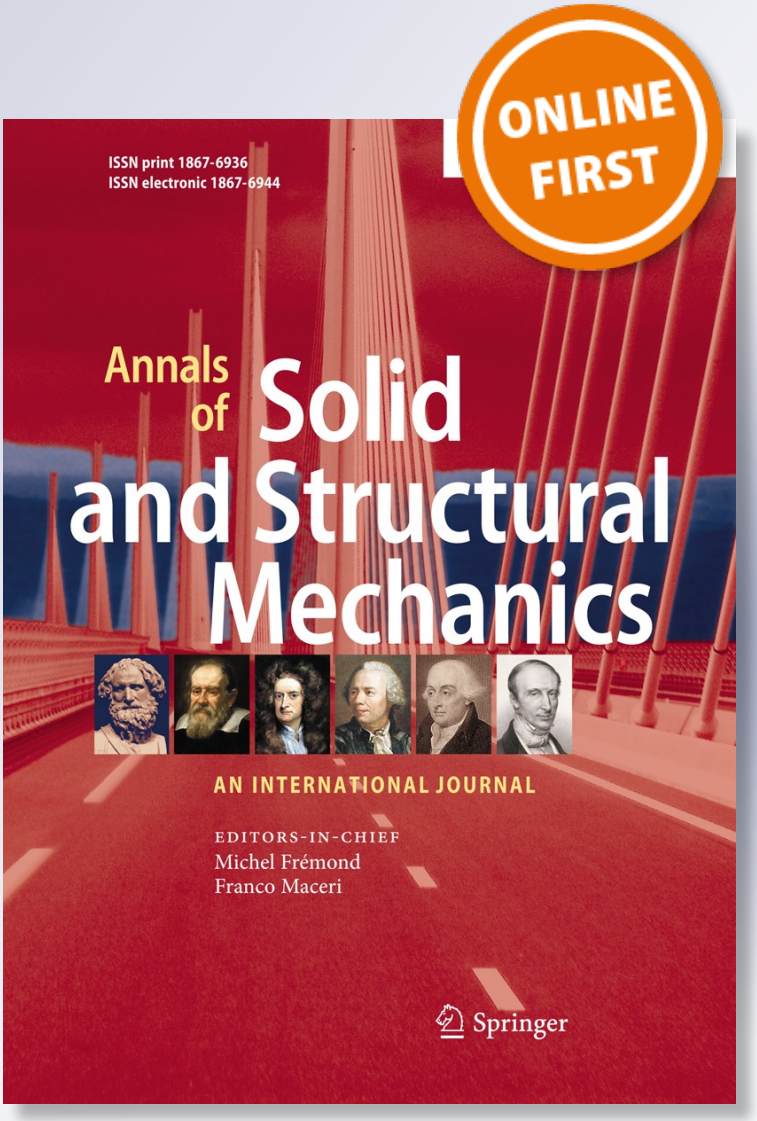

Springer

Ann. Solid Struct. Mech.
DOI 10.1007/s12356-012-0028-x

ORIGINAL ARTICLE

Comparison and critical analysis of invariant-based models with respect to their ability in fitting human aortic valve data

F. Auricchio · A. Ferrara · S. Morganti

Received: 3 November 2011 / Accepted: 8 September 2012

Abstract With the increase of life expectancy and population average age, heart valve diseases have become more frequent, representing an always increasing percentage among cardiovascular diseases, which are the predominant cause of death in the western country. For this reason, research activities within such a context and, in particular, computer-based predictions of valve behavior are strongly motivated. Consequently, the study of the tissue mechanical response and the constitutive relationships for modeling material behavior represent crucial a aspect to be investigated in order to perform realistic simulations. The mechanical response of the aortic valve tissue depends on the contribution, composition, and interaction of different constituents, such as collagen fibers and elastin network. Accordingly, constitutive laws including non-linearity and anisotropy are necessary. Clearly, the complexity of a constitutive model increases more as it takes into account the histological structure of the tissue. Numerous constitutive models have been developed to describe arterial tissue, but relatively few models have been calibrated specifically for the aortic valve. This study focuses on the investigation of constitutive models so far proposed in the literature which could be suitable to capture the mechanical behavior of the aortic valvular tissue. To make the right choice, the comparison between these constitutive models is done in terms of the fitting quality achieved with respect to human aortic valve data proposed in the literature. For this purpose, an optimization technique based on the nonlinear least square method is used. The obtained material parameters could be later used in finite element analysis adopted, in this last decade, as an innovative approach to support the operation planning procedure and the design of artificial grafts.

Keywords Aortic valve · Mechanical properties · Anisotropy · Constitutive law · Parameter identification

F. Auricchio · A. Ferrara (✉) · S. Morganti
Dipartimento di Ingegneria Civile e Architettura (DICAr), Università degli Studi di Pavia, Via Ferrata, 1-27100 Pavia, Italy
e-mail: anna.ferrara@unipv.it

F. Auricchio
Istituto di Matematica Applicata e Tecnologie Informatiche "Enrico Magenes" (IMATI), CNR, Pavia, Italy

F. Auricchio
Centro di Simulazione Numerica Avanzata (CeSNA), IUSS, Pavia, Italy

1 Introduction

Cardiovascular diseases represent a major worldwide health care issue. In particular, a considerable amount of diseases is represented by heart valve failure due to increasing life expectancy and population average age. A current approach in surgical treatments is heart valve replacement using prosthetic, mechanical or biological, valves [1–4]. In this last decade, the use of computational tools to investigate heart and valvular mechanics has gradually grown and, in particular, finite element analysis –FEA—has been frequently adopted as an innovative approach to support the operation planning procedure [5–8] as well as the design of artificial grafts [9].

In the past, phenomenologically-based models with exponential and power-law functions were used to describe the (macroscopic) material response of various soft biological tissues [10–13]. Even though these strain-energy functions (SEFs) are able to capture the nonlinear stiffening response, they have a significant limitation due to

Published online: 25 September 2012

material parameters having no direct physical or morphological meaning.

With the aim of moving towards the real and patient-specific characterization of human aortic valve tissues, appropriate constitutive materials models—motivated by tissue histology—could be considered. In modeling heart valve biomechanics, existing approaches at different scale length (organ-, tissue-, cell- and molecular-scale) have been reviewed by Weinberg et al. [14] which also emphasized the necessity of using multi-scale modeling approaches to capture the general heart valve behavior and to overcome some limitations related with the employment of phenomenological laws. However, the complexity of a constitutive model increases with the tissue histological features such as fiber crimp, fiber arrangement, collagen content and multi-layered organization [15–19], so that a trade-off between structural accuracy as well as mathematical and computational simplicity should be seek.

With the main goal of quantifying the material properties of human aortic valve, we focus on constitutive models at tissue-scale. Neglecting temperature as well as viscous and time-dependent effects, it is possible to model soft tissue mechanics in the context of nonlinear hyper-elasticity [20]. Consequently, the constitutive law of the aortic valve tissue may be obtained by derivation of a strain-energy function (SEF) with respect to the deformation measurements.

In agreement with the invariant theory [21, 22], the anisotropy of soft tissues may be included in the SEF through invariants of structure tensors defined in terms of the preferred directions. In the literature, two main invariant-based formulations have been developed and used for a variety of soft tissues. These approaches differ by whether the collagen orientation is modeled as a continuous distribution over a range of fiber orientations, or as a discrete distribution in which all fibers are aligned along one or two primary directions.

A first step toward a more realistic description taking into account fiber dispersion was addressed to model connective tissue by Lanir [23], to model arteries by Gasser et al. [24] and to reproduce the mechanical behavior of aortic valves leaflets by Billiar and Sacks [25], Sacks and Sun [26] and Driessen et al. [27]. On the contrary, the invariant-based model with a strong collagen fiber orientation was discussed, for example, in the works of Humphrey and Yin [28, 29] for the myocardium, of May-Newman and Yin [30, 31] for the mitral leaflet, of Hayashi and Holzapfel et al. for the artery [32, 33].

If on one hand, the discrete fiber distribution is a major constitutive assumption leading to poor model prediction, on the other hand analytic and computational simplicity of the stress tensor and the material stiffness are achieved. Moreover, it is extremely hard to find in the literature precise data on angular fiber distribution in human while it is definitely easier to find out stress-strain curves of uniaxial and biaxial tests. Consequently, in dealing with the decision to refer only on human experimental data as well as to avoid constitutive models numerically cumbersome, we have considered models with a strong angular fiber alignment.

In addition, to our knowledge, no specific constitutive models for the aortic root have been presented in the literature. In fact, most numerical studies have oversimplified or overlooked the non-linear anisotropic property of human aortic root; in some works the mechanical properties of the aortic root have been considered identical to those of the adjacent ascending aorta [5, 34, 35]. However, it has been demonstrated in the literature [36–38] that the human aortic root anatomy and its mechanical material properties have significant impact on leaflet stress, strain and coaptation becoming crucial aspects to be taken into account to improve the computational model quality.

Finally, in dealing with model calibrations, an important aspect to be considered is that the material parameters of most constitutive models are calibrated on porcine data. On one hand, the employment of porcine data is motivated by the abundance of porcine experimental data on both the aortic valve leaflets [25, 39–43] and the aortic valve sinuses [40, 44–46] in comparison with humans. On the other hand, porcine valves are frequently employed for replacements in humans with bioprosthetic valves [47–49]. However, morphological as well as material and structural differences [50–53] have been evidenced suggesting that the validity of using porcine data in clinical trials may be questionable.

Keeping in mind the previous considerations, this paper deals with the constitutive modeling of human aortic valve distinguishing between human aortic leaflets and sinuses. To our knowledge in the literature there is a lack of works collecting and comparing different constitutive models in order to predict the mechanical behavior of human aortic valve. Consequently, we mainly propose a comparison of different invariant-based strain-energy functions available in the literature with respect to their ability in fitting available human experimental data. Accordingly, the major objectives of this study are: (1) to calibrate through a numerical optimization scheme the considered constitutive models with respect to a specific set of experimental data; (2) to determine the optimal model which provides the best fit.

In the following, we briefly present the organization of the paper. After the introduction, Sect. 2 starts with a short description of the histological and mechanical experimental evidence. Then, the invariant-based constitutive models (typically used for soft tissues) as well as the optimization method used to identify the material parameters are

discussed. The data and the fitting results are presented in Sect. 3, whereas our discussion and conclusion in Sect. 4.

2 Materials and methods

2.1 Histological and mechanical evidences

The *aortic valve* is located between the left ventricle and the ascending aorta and allows the passage of blood from the left ventricle to the aorta preventing flow in the reverse direction [54, 55]. The aortic valve consists of the *root* and of three flexible *leaflets* which are attached to the root at one edge and are free to move at the other one, see Fig. 1a. Behind each leaflet the aortic root bulbs into three cavities called *sinuses of Valsalva* to form the beginning of the ascending aorta. The three cavities are labeled as: left coronary sinus (LCS), non-coronary sinus (NCS), and right coronary sinus (RCS).

For details on the anatomy and histology of the aortic valve, we remand the reader to devoted studies [56–60], whereas in the following we highlight only the major structural constituents. At microscopical level, the aortic valve tissue appears as a fibrous network containing mainly collagen fibrils embedded in a ground matrix consisting of elastin, proteoglycans and water.

Elastin and collagen are the mainly components determining the mechanical behavior of the tissue. While elastin load-bearing at low stresses and at small strains, collagen fibers providing highest stiffness and tensile strength at higher stresses, [61–63]. The progressive recruitment to the resistance of collagen fibers (during a loading process) leads to the J-shaped stress-strain curve typical of soft tissues. The concentration and the structural arrangement of the tissue constituents are different within the aortic leaflets and sinuses according to their specific functions [57].

Briefly, the aortic sinuses are composed of three layers as the adjacent ascending aorta: *tunica intima*, *tunica media* and *tunica adventitia* [56], but with a wall thickness significantly thinner than the ascending aorta [44]. The structure of the Valsalva sinuses wall is also similar to that of the aortic wall in terms of composition with elastic lamellae alternated with smooth muscle cell layers and collagen fibers [59]. Schrief et al. [64] have recently evidenced two distinct (helically distributed) fiber families in the aortic wall so that, due to the structural continuity between aortic root and aorta, it may be acceptable to assume a similar fiber organization in the aortic root, see Fig. 1b.

On the other hand, the aortic leaflets consists of three distinct layers: the *ventricularis*, the *spongiosa*, and the *fibrosa* [65–68]. Histological evidences [53] reveal that in human leaflets (contrary to porcine) the fibrosa is much thicker than both the spongiosa and ventricularis, with an high content of collagen fibers highly aligned along the circumferential direction, see Fig. 1c. Such an evidence assigns to this layer nonlinear and anisotropic properties with an higher stiffness in the circumferential direction than in the radial one. Recently, Martin and Sun [53] have evidenced that human leaflets tissue is much stiffer than the corresponding porcine tissue with (circumferential) stress–strain curves without an evident transition zone from the low-toe region to the stiffer one.

2.2 Constitutive model

Constitutive models based on the theory of nonlinear hyper-elasticity are commonly used to describe the mechanical properties of soft biological tissues as the aortic valve tissue. In this context, the constitutive laws are described in terms of a strain-energy function per unit reference volume [24, 28, 33, 70].

Following the invariant formulation proposed by Spencer [21, 22], the SEF is expressed as function of the three *isotropic* invariants, I_1, I_2, I_3, of the right Cauchy-Green strain tensor $\mathbf{C} = \mathbf{F}^T\mathbf{F}$ (with $\mathbf{F}$ the deformation gradient):

$$I_1 = \mathrm{tr}\mathbf{C}, \qquad I_2 = \frac{1}{2}\left[I_1^2 - \mathrm{tr}\mathbf{C}^2\right], \qquad I_3 = \det\mathbf{C}, \tag{1}$$

and of additional *anisotropic* invariants defined in terms of $\mathbf{C}$ and of the preferred directions.

In particular, for soft tissues reinforced by one-fiber family (*transversely isotropic*), the additional invariants are:

$$I_4 = \mathbf{C} : \mathbf{a}_0 \otimes \mathbf{a}_0, \qquad I_5 = \mathbf{C}^2 : \mathbf{a}_0 \otimes \mathbf{a}_0, \tag{2}$$

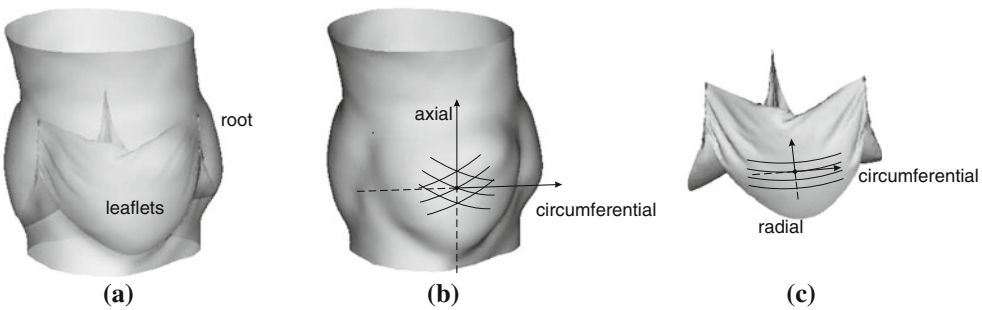

Fig. 1 **a** Human aortic valve; **b** aortic root with a strong schematic representation of the two collagen fiber-families symmetrically arranged around the major axes [56, 59]; **c** aortic leaflets with a strong schematic representation of the single collagen fiber-family highly oriented in the circumferential direction [53, 69]

with $\mathbf{a}_0$ a unit vector that detects the main orientation of the fiber family in the reference configuration, and $\mathbf{a}_0 \otimes \mathbf{a}_0$ the structural tensor associated with $\mathbf{a}_0$. It is worth noting that I_4 represents the square of the stretch along the preferred direction, whereas I_5 registers shear deformations [71, 72].

For soft tissues reinforced by two-fiber families (the second denoted by $\mathbf{b}_0$), other two additional invariants are introduced:

$$I_6 = \mathbf{C} : \mathbf{b}_0 \otimes \mathbf{b}_0, \qquad I_7 = \mathbf{C}^2 : \mathbf{b}_0 \otimes \mathbf{b}_0, \tag{3}$$

as well as a coupling invariant I_8 related to the pair of the two preferred directions ($\mathbf{a}_0$, $\mathbf{b}_0$):

$$I_8 = \mathbf{a}_0 \cdot \mathbf{b}_0[\mathbf{C} : \mathrm{sym}(\mathbf{a}_0 \otimes \mathbf{b}_0)], \tag{4}$$

with the terms $\mathbf{a}_0 \cdot \mathbf{b}_0$ included in Eq. (4) to ensure that I_8 is not affected by reversal of either $\mathbf{a}_0$ or $\mathbf{b}_0$. Merodio and Ogden [73] have evidenced that the coupling invariant I_8 have a destabilizing effect on the stress-deformation and ellipticity of the governing equations, so that it should be considered carefully in the construction of constitutive models.

As explained firstly by Humphrey and Yin [28] and later by Holzapfel and Ogden [74], if all the invariants are included in the SEF it is difficult to describe the most common features of anisotropic materials. In order to overcome this drawback, the invariants not strictly needed are omitted from the constitutive law. For biological materials the influence of the fibers on the strain energy is frequently assumed to be due to the fiber stretches [15, 75].

Then, for incompressible materials ($I_3 = \det \mathbf{C} = 1$) reinforced by one-fiber family, the SEF and the Cauchy stress tensor are given by:

$$\begin{aligned} &\Psi = -p(I_3 - 1) + \Psi(I_1, I_4), \\ &\boldsymbol{\sigma} = -p\mathbf{I} + 2\Psi_1\mathbf{B} + 2\Psi_4(\mathbf{a} \otimes \mathbf{a}), \end{aligned} \tag{5}$$

with $\Psi_a = \partial\Psi/\partial I_a$ ($a = 1, 2, 4, 6$) and p a Lagrange multiplier determined from boundary conditions. The vector $\mathbf{a} = \mathbf{F}\mathbf{a}_0$ is the *push forwards* of $\mathbf{a}_0$ under the action of $\mathbf{F}$, whereas the tensor $\mathbf{B}$ is the left Cauchy-Green strain tensor $\mathbf{B} = \mathbf{F}\mathbf{F}^T$.

The counterpart of Eq. (5) for material reinforced by two-fiber families is obtained by including the dependence on the invariant I_6 as follows:

$$\begin{aligned} &\Psi = -p(I_3 - 1) + \Psi(I_1, I_4, I_6), \\ &\boldsymbol{\sigma} = -p\mathbf{I} + 2\Psi_1\mathbf{B} + 2\Psi_4(\mathbf{a} \otimes \mathbf{a}) + 2\Psi_6(\mathbf{b} \otimes \mathbf{b}). \end{aligned} \tag{6}$$

with $\mathbf{b} = \mathbf{F}\mathbf{b}_0$ the *push forwards* of $\mathbf{b}_0$ under the action of $\mathbf{F}$. For further details on the components of the stress tensor in Eq. $(5)_2$ and Eq. $(6)_2$, we remand to Appendix.

As highlighted in [33], the previous cited constitutive model formulation may be generalized to a multi-layered formulation for accurate modeling of aortic valve, but this demand the knowledge of structural and mechanical information on each tissue layers. Since such experimental data are not available in the literature for human valvular tissue, we assume the material homogeneous through the thickness.

2.3 Invariant-based strain-energy functions

In the following, we present the strain-energy functions that we will use to model the mechanical behavior of human aortic sinuses as well as human aortic leaflets.

With respect to human aortic sinuses, we decide to use two-fiber family models, motivated by the structural similarities between aortic sinuses and ascending aorta [56, 59, 64]. In particular, we consider the SEF of Holzapfel et al. [33] (typically known as HGO model) which proved to be accurate for the arterial tissue. This model is written in a split form wherein the contribution of elastin is described by the neo-Hookean potential, whereas the contribution of the two collagen fibers by two exponential functions (written in terms of the anisotropic invariants I_4 and I_6, respectively). It is worth noting that this model considers the two-fiber families mechanically equivalent, i.e. $\Psi_4 = \Psi_6$ and then symmetrically oriented around to the major axis. It is worth noting that the fiber orientation angles $\pm\beta$ hide in the expressions of the invariants I_4 and I_6, see Appendix for calculation details.

On the other hand, with respect to human aortic leaflets, we compare the transversely isotropic strain-energy functions listed in Table 1 according to their expression and application field. In particular, the potentials of May-Newman and Yin [31] and Prot et al. [76] consist of a single-exponential term which takes into account the interaction between elastin and collagen fibers by the dependence on both invariants I_1 and I_4.

Subsequently, these models have been modified by Weinberg and Kaazempur-Mofrad [77] and Prot et al. [78] by adding the neo-Hookean potential. As highlighted by Weinberg and Kaazempur-Mofrad [77], the need to include such a separate term is due to maintain positive definiteness of the stiffness matrix at low strains. In our work, we accept the suggestion only for fitting purposes and investigate the effects of this modification on the results. It is worth noting that in the study of Weinberg and Kaazempur-Mofrad [77] the material was considered compressible. Hence, we have adapted such an expression for our incompressibility assumption. In particular, the volumetric contribution has been replaced by the term $-p(I_3 - 1)$ and the isochoric one re-written in terms of the invariants of $\mathbf{C}$ rather than $\overline{\mathbf{C}}$.

The potential proposed by Humphrey and Yin [28] is also considered in our study. This model consists of two-exponential expressions, one written in terms of I_1 and

Table 1 Transversely isotropic strain-energy functions available in the literature and listed according to their functional form

Author	Anisotropic strain-energy function	Application
Holzapfel et al. [33]	$c(I_1-3)+c_0\left\{\exp\left[c_2(I_4-1)^2\right]-1\right\}+c_0\left\{\exp\left[c_2(I_6-1)^2\right]-1\right\}$	Arteries
Humphrey—α	$c\{\exp[c_1(I_1-3)]-1\}+c_0\left\{\exp\left[c_2(I_4-1)^2\right]-1\right\}+c_0\left\{\exp\left[c_2(I_6-1)^2\right]-1\right\}$	
Author	**Transversely isotropic strain-energy function**	**Application**
May-Newman and Yin [31]	$c_0\left\{\exp\left[c_1(I_1-3)^2+c_2\left(\sqrt{I_4}-1\right)^4\right]-1\right\}$	Mitral leaflets
May-Newman et al. [41]		Aortic leaflets
Prot et al. [76]	$c_0\left\{\exp\left[c_1(I_1-3)^2+c_2(I_4-1)^2\right]-1\right\}$	Mitral leaflets
Weinberg and Kaazempur-Mofrad [77][a]	$c(I_1-3)+c_0\left\{\exp\left[c_1(I_1-3)^2+c_2\left(\sqrt{I_4}-1\right)^4\right]-1\right\}$	Mitral leaflets
Prot et al. [78]	$c(I_1-3)+c_0\left\{\exp\left[c_1(I_1-3)^2+c_2(I_4-1)^2\right]-1\right\}$	Mitral leaflets
Humphrey and Yin [28]	$c\{\exp[c_1(I_1-3)]-1\}+c_0\left\{\exp\left[c_2\left(\sqrt{I_4}-1\right)^2\right]-1\right\}$	Myocardium
Humphrey—α	$c\{\exp[c_1(I_1-3)]-1\}+c_0\{\exp[c_2(I_4-1)^\alpha]-1\}$	

[a] The SEF [77] formulated for a compressible material has been adapted according to the incompressibility assumption

the other in terms of I_4, in order to consider separately the contribution of elastin and collagen fibers. Subsequently, Humphrey et al. [75] suggested a polynomial expression with a coupling term as better descriptor of the behavior of myocardium. In our calibrations the SEF of Humphrey et al. [75] will be disregarded because of, following Fung et al. [11], it is preferable for fitting purposes an expression with a smaller number of unknown material parameters.

Finally, since the model of Holzapfel et al. [33] is implemented in different FE commercial codes, its transversely isotropic form (with only the terms in I_1 and I_4, see Table 1) is also considered and compared with the others. Moreover, we propose to modify the model of Humphrey and Yin [28] combining its original formulation with the model of Holzapfel et al. [33] (i.e., removing the root square of I_4) and considering also the exponent of the I_4-term (α in Table 1) as an unknown parameter. It is straightforward to generalize the proposed model to the anisotropic case, see Table 1.

2.4 Optimization method

The estimation of material parameters for a given constitutive model is a major topic in soft tissue mechanics. As largely done in the literature [32, 79, 80], the adopted optimization procedure is based on the non linear least squares method.

Since more of the considered experimental data refer to biaxial testing, in the following we particularize the adopted procedure for this test typology. With respect to planar biaxial tests, the indirectly measured kinematic quantities are the in-plane stretches λ_1 and λ_2, whereas $\lambda^3=\lambda_1^{-1}\lambda_2^{-1}$ for the incompressible condition.

The directly measured static quantities are the in-plane loads f_1, f_2 applied to the lateral edges of the sheet. From these quantities the in-plane components of the Cauchy stress tensor, $\sigma_{11}^{\exp}$ and $\sigma_{22}^{\exp}$ are obtained, where the superscript "exp" stands for experiment:

$$\sigma_{11}^{\exp}=\frac{f_1}{L_2H}\cdot\lambda_1,\qquad \sigma_{22}^{\exp}=\frac{f_2}{L_1H}\cdot\lambda_2, \tag{7}$$

with L_1, L_2 the in-plane dimensions and H the thickness of the specimen in the reference configuration. The normal stress $\sigma_{33}^{\exp}=0$ for the plane stress assumption.

Given the pair of stretches (λ_1,λ_2) and the strain-energy function $\Psi(\kappa,\lambda_1,\lambda_2)$, with κ the unknown material parameter set, the theoretical stresses, σ_{11}^{Ψ} and σ_{22}^{Ψ}, are computed by derivation of the strain-energy function with respect to the strain measures, where the superscript Ψ script stands for theoretical value.

An explicit expression of the stress components σ_{11}^{Ψ} and σ_{22}^{Ψ} is given in Appendix, whereas in a more compact form, we can write:

$$\sigma_{11}^{\Psi}=\sigma_{11}^{\Psi}(\kappa,\lambda_1,\lambda_2),\qquad \sigma_{22}^{\Psi}=\sigma_{22}^{\Psi}(\kappa,\lambda_1,\lambda_2). \tag{8}$$

The standard minimization technique requires the definition of the objective function χ^2 as the squared sum of the residuals, i.e., the difference between the experimental stress data and the corresponding theoretical values:

$$\chi^2(\kappa)=w_1^2\sum_{a=1}^{p}\left[\left({\sigma_{11}}_a^{\Psi}-{\sigma_{11}}_a^{\exp}\right)^2\right]+w_2^2\sum_{a=1}^{p}\left[\left({\sigma_{22}}_a^{\Psi}-{\sigma_{22}}_a^{\exp}\right)^2\right], \tag{9}$$

with p the number of data points.

The weighting factors w_1 and w_2 are set to the mean value of the stresses ${\sigma_{11}}_a^{\Psi}$ and ${\sigma_{22}}_a^{\Psi}$.

They are introduced in order to scale properly the two residual terms $\left({\sigma_{11}}_a^{\Psi} - {\sigma_{11}}_a^{\exp}\right)^2$ and $\left({\sigma_{22}}_a^{\Psi} - {\sigma_{22}}_a^{\exp}\right)^2$ so that they equally affect the minimization process. Hence, the effect of w_1 and w_2 is felt when the two residual terms have different order of magnitude.

The minimization problem becomes:

$$\begin{cases} \min\limits_{\kappa} \chi^2(\kappa), \\ \text{subjected to:} \quad \kappa \in K, \end{cases} \tag{10}$$

whit $K = \{\kappa: \kappa^- \leq \kappa \leq \kappa^+\}$ the solution space and κ^- and κ^+ the lower and upper bounds for the material parameters, respectively. In our computations, the fixed bounds K are those necessary to define the domain of the identified strain-energy functions and to discard the non-physical solutions a priori. The quality of the best solution κ^* is validate computing proper error measures, such as the normalized mean square root error (NRMSE) adopted, for example, in [81]:

$$\text{NRMSE} = \sqrt{\frac{\chi^2}{p-q}} \cdot \frac{1}{\sigma_{\text{ref}}}, \tag{11}$$

with q the number of parameters. The quantity σ_{ref} is the sum of all Cauchy stresses for each data point divided by the number of all data points:

$$\sigma_{\text{ref}} = \frac{1}{p} \cdot \sum_{a=1}^{p} \left({\sigma_{11}}_a^{\exp} + {\sigma_{22}}_a^{\exp}\right). \tag{12}$$

Commercial codes—based on some suitable modification of the Newton method—are used to accomplish the minimization. These iterative techniques require an initial guess κ_0 for the solution and stop when appropriate stopping criteria are satisfied, i.e., when some quantities become less than a threshold value. However, these algorithms are not able to distinguish global and local minima, so that the solution is strong dependent on the initial guess κ_0 [80, 82].

In order to overcome this undesirable occurrence, a global search algorithm (i.e., a method able to identify the global minimum in the solution space) has been used in this study. In particular, we have developed a procedure in MATLAB (The Mathworks, Natick, MA, USA) to implement the objective function (9) for each considered strain-energy function, whereas the minimization problem (10) has been solved using the *MultiStart* solver available in the Global Optimization Toolbox of Matlab. In order to search the global minimum, the solver works by starting a local solver from multiple start points. We choose as local solver the standard function *lsqcurvefit* available in the Matlab Optimization Toolbox, whereas the start points are randomly generate and uniformly distributed within the bounds $\mathcal{K}$ by passing a *RandomStartPointSet* object to the solver.

With respect to the local solver *lsqcurvefit*, the iterations can stop when: (1) the maximum number of iterations MaxIter is performed; (2) the Newton step becomes less than a threshold value, TolX; (3) the infinity norm of the estimated gradient ∇ of the objective function χ^2 is less than a threshold value, TolFun. For the local solver, we consider the default values MaxIter = 1,000, TolX = 10^{-6} and TolFun = 10^{-6}.

With respect to the global solver *MultiStart*, we fix TolX = 10^{-2} and TolFun = 10^{-2}, i.e., two solutions are considered identical by the global solver if they are within TolX = 10^{-2} distance of each other and they have objective function values within TolFun = 10^{-2} of each other. Finally, for improving results, we run *MultiStart* solver for a more large number of start points (for example 200) than the default value of 50.

It is worth noting that the fiber orientation angles $\pm\beta$ could be identified through adequate techniques [69, 83, 84] being a micro-structural parameter. On one hand, with respect to leaflets, we have assumed $\beta = 0°$ because of the strong alignment of collagen fibers along the circumferential direction. On the other hand, we consider the angle β as an unknown material parameter since no precise data are available in the literature.

3 Results

In this section, we present the results of the fitting procedure obtained for each investigated constitutive model and for each set of experimental data distinguishing the case of human aortic leaflets and human aortic sinuses. The comparison between the investigated strain-energy functions is made up in terms of the quality of the fitting results.

It is worth noting that both the strain-energy functions and the experimental data used in this study are available in the literature. In particular, with respect to aortic sinuses, the biaxial stressing data of Martin et al. [52] are taken into account; whereas with respect to aortic leaflets, we consider the uniaxial data of Stradins et al. [85] and the more recent biaxial stressing data of Martin and Sun [53].

3.1 Aortic valve sinuses

3.1.1 Fitting results on Martin et al. [52] data

Biaxial testing was carried out on fresh-frozen human aortic sinuses utilizing tension-controlled test protocols according to the methods presented in Sacks and Sun [26]. The experimental results highlight nonlinear anisotropic stress–strain responses in both the circumferential and

longitudinal directions. Although the shift between the two curves is little, all specimens are stiffer in the circumferential direction that in the axial one.

The (equi-) biaxial data of Martin et al. [52] are calibrated by using the SEFs of Holzapfel et al. [33] and the anisotropic counterpart of the proposed modified model (Humphrey—α), see Table 1. The obtained constitutive material parameters and the related normalized mean square root error–*NRMSE*—are summarized in Table 2, for the left coronary sinus (LCS), non-coronary sinus (NCS), and right coronary sinus (RCS).

Comparing the results, we note that each model provide similar material parameters for LC-, NC-, and RC-sinuses, respectively, and that the *NMRSE* error is very similar between the two considered models. Moreover, the two models provide also similar β-orientation angles with values inside the range observed by Schriefl et al. [64] for human aortic wall. It should be noted that the found β-angles are in agreement with the little shift between the circumferential and axial experimental curves (i.e., values of stretches λ_1 and λ_2 very close for given equibiaxial stresses, $\sigma_{11} = \sigma_{22}$). In fact, Eq. (A.4) shows that this occurrence takes place when β is close to 45°.

Finally, the predicted stress-strain curves plotted in Fig. 2 point out that the proposed modified model Humphrey—α better captures the trend of the data than the SEF of Holzapfel et al. [33] at low and higher stresses.

3.2 Aortic valve leaflets

3.2.1 Fitting results on Stradins et al. [85] data

The obtained constitutive material parameters and the related *NRMSE*, are listed in Table 3, whereas the fitting results are shown in Fig 3.

Comparing the investigated SEFs, we note that the model of May-Newman et al. [41] achieves the worst fit, $NMRSE = 0.3058$, whereas the model proposed by Humphrey and Yin [28] provides the best value of *NMRSE* equal to 0.15. The remaining potential of Prot et al. [76] and Holzapfel et al. [33] give a slight higher value of the error than the best one, i.e., $NMRSE = 0.1635$ and $NMRSE = 0.1751$ respectively. Moreover, as shown in Table 3, the neo-Hookean term improves the fit quality in both the models of May-Newman et al. [41] and Prot et al. [76]. In fact, the error *NRMSE* decreases from 0.3058 to 0.2107 for the modified model [31] labeled as Weinberg and Kaazempur-Mofrad [77], and from 0.1635 to 0.1468 for the modified model [76] labeled as Prot et al. [78].

However, the error *NRMSE* reflects only the overall quality of the fitting procedure. A closer inspection of Fig. 3 highlights that, with respect to the circumferential data, the model of May-Newman and Yin [31] underestimates the data in a considerable range of deformation (0–15%) whereas the others capture fairly well the experimental data above the stress value of 0.5 MPa. On the other hand, with respect to the radial data, only the model of Holzapfel et al. [33] fails providing an almost straight response due to the single dependence of the radial stress σ_{22}^{Ψ} on the first derivative $\Psi_1 = c$.

On the contrary, the split exponential term in the model of Humphrey and Yin [28] provides a more accurate estimation of the radial data. This occurrence appears consistent with the evidences of Milnor [86] on the nonlinear behavior of the elastin. Finally, our results reflect the strong dependence of the circumferential stress σ_{11}^{Ψ} on the I_4-term, while the I_1-term, although included differently in the potentials, does not affect the circumferential response, so that split strain-energy functions without interaction terms appear preferable.

Table 2 Calibrations of the SEFs of Holzapfel et al. [33] and the proposed model with $\alpha = 2$ with respect to the experimental data by Martin et al. [52] (aortic valve sinuses)

Ψ	Sample	Material parameters						NRMSE
		c (kPa)	c_0 (kPa)	c_1 (–)	c_2 (–)	β (°)	α	
Holzapfel et al. [33]	LCS	12.82	0.35	–	84.52	44.89	2	0.0120
	NCS	12.00	0.34	–	53.70	44.70		0.0177
	RCS	14.86	0.26	–	116.8	44.68		0.0167
	mean	13.23	0.32	–	85.01	44.75	2	0.0169
	±SD	1.47	0.05	–	31.56	0.12		0.0045
Humphrey—α	LCS	16.04	0.25	1.05	410.4	44.82	2	0.0113
	NCS	0.77	9.31	21.26	1.50	40.57		0.0157
	RCS	0.95	8.63	35.52	1.39	39.01		0.0109
	mean	5.92	6.06	19.28	137.75	41.47	2	0.0126
	±SD	8.76	5.05	17.32	236.08	3.01		0.0027

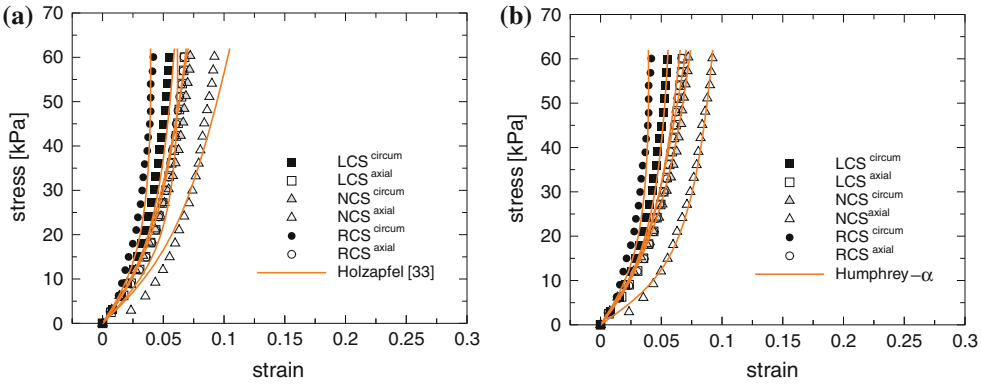

Fig. 2 Fitting results on the experimental data of Martin et al. [52] (aortic valve sinuses) by using the SEFs of: Holzapfel et al. [33] and the proposed model with $\alpha = 2$

Table 3 Calibrations of the SEFs listed in Table 1 with respect to the experimental data of Stradins et al. [85] (aortic valve leaflets)

Ψ	Material parameters				α	NRMSE
	c (MPa)	c_0 (MPa)	c_1 (–)	c_2 (–)		
May-Newman and Yin [31]	–	16.01	0.07	3.66	–	0.3050
Prot et al. [76]	–	0.188	5.07	2.33	–	0.1635
Weinberg et al. [77]	0.249	17.06	0.00	3.20	–	0.2106
Prot et al. [78]	0.105	0.118	4.50	3.21	–	0.1477
Humphrey et al. [28]	0.022	0.062	5.81	24.97	2	0.1500
Holzapfel et al. [33]	0.222	0.067	–	4.78	2	0.1751
Humphrey—α	0.041	14.71	3.83	0.08	3	0.0898

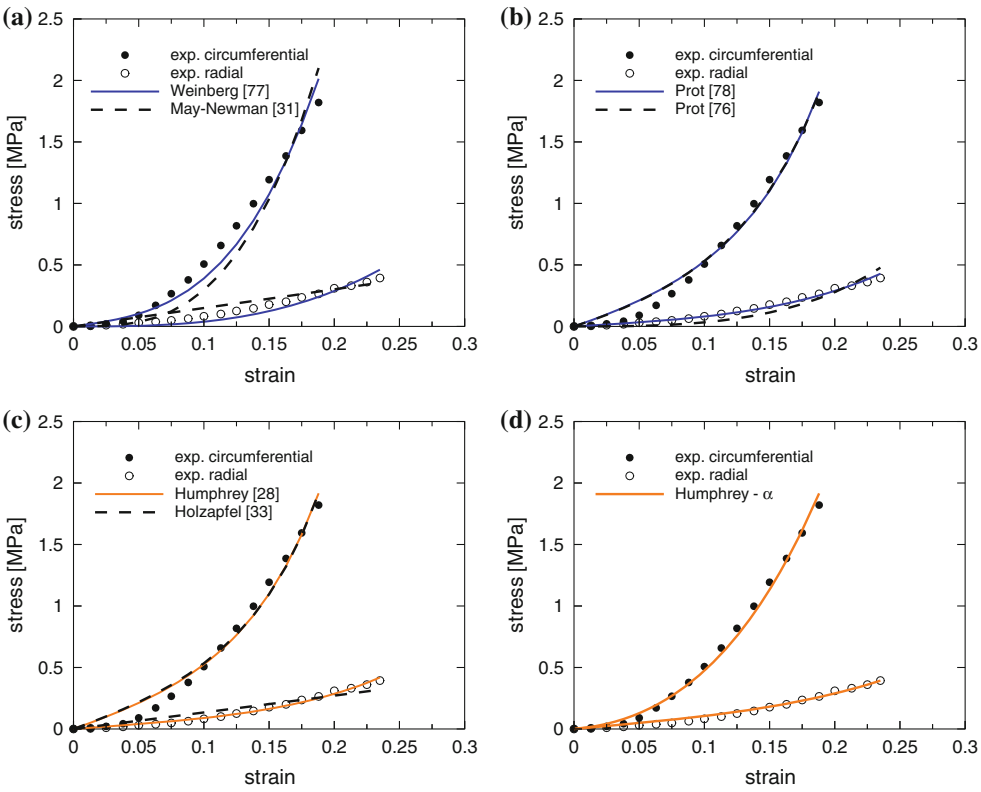

Fig. 3 Fitting results on the experimental data of Stradins et al. [85] (aortic valve leaflets) by using the SEFs of: May-Newman and Yin [31] and Weinberg and Kaazempur-Mofrad [77]; Prot et al. [76, 78] Humphrey and Yin [28] and Holzapfel et al. [33]; and the proposed modified model with $\alpha = 3$

Except for the model of Weinberg and Kaazempur-Mofrad [77], all the investigated SEFs are not able to capture the circumferential response at low stress values (<0.5 MPa). The proposed modified model Humphrey—α is able to accurately capture both the radial and circumferential responses at low and higher stress values.

However, the previous discussion is based on calibrations performed on uniaxial tensile data, which alone are insufficient for approximating the anisotropic behavior of soft tissues, and then rarely used to define constitutive relations. In some experimental studies [74, 81, 87, 88], uniaxial tensile tests along two different directions are carried out, but as evidenced for example by Holzapfel et al. [81] different indication on the tissue anisotropy could be produced since the integrity of the tissue is altered although the strips are taken from neighboring locations.

3.2.2 Fitting results on Martin and Sun [53] data

Biaxial testing was carried out on fresh-frozen human aortic leaflets utilizing tension-controlled test protocols according to the methods presented in Sacks and Sun [26]. All of the tested samples exhibit nonlinear anisotropic behavior with higher stiffness in the circumferential direction than in the radial one. In addition, the circumferential stress-strain curves have not an evident transition zone from the low-toe region to the stiffer zone. This mechanical evidence is in agreement with the evidenced high content of collagen fibers which highly aligned along the circumferential direction.

Following the considerations in Sect. 3.2.1, we compare the SEFs used to fit the uniaxial data, except for the model of Holzapfel et al. [33] because of it provides an almost straight response in the radial data direction. The obtained constitutive material parameters and the related normalized mean square root error, *NRMSE*, are listed in Table 4 distinguishing left coronary leaflet (LCL), non-coronary leaflet (NCL), and right coronary leaflet (RCL).

A closer inspection of Table 4 highlights that the trend of the error measure *NRMSE* is the same for each constitutive model: the highest values are achieved by LCL samples while the lowest by RCL. Although no significant differences are found between the error measures of each investigated model, the lowest *NRMSE* values are provided by the proposed Humphrey—α model (in particular for LCL and RCL specimens). On the contrary, the model of Weinberg and Kaazempur-Mofrad [77] gives the highest *NRMSE* values (in particular for LCL specimens).

These considerations are enhanced by the predicted stress-strain curves plotted in Fig. 4. In fact, almost all investigated SEFs reproduce well the trend of the experimental data. The only exceptions evidenced by a closer inspection of the plots are: the models of Weinberg and Kaazempur-Mofrad [77] and of Prot *et al*. [78] for the LCL specimen in the radial direction. In particular, Weinberg and Kaazempur-Mofrad [77] model fails at low and higher stress values whereas the Prot et al. [78] model only at low stress values (<15 kPa). On the contrary, the model of Humphrey et al. [28] and, especially, the proposed modified model Humphrey—α capture both the radial and circumferential responses at low and higher stress values for the LCL, NCL and RCL specimens.

4 Discussion

The knowledge of aortic valve mechanical properties as well as the ability to describe their mechanical response by using appropriate constitutive models is crucial for understanding the onset, progression and treatment of the common valvular heart diseases, such as valve failure and aortic stenosis. The ability to characterize the mechanical properties of aortic valve tissues is also important in the development of aortic valve bio-prostheses since the mechanical properties of replacement materials should mimic those of native tissues.

Accordingly, it appears of paramount importance to consider constitutive models motivated by the tissue histology as well as to calibrate the constitutive material parameters on data of human aortic valve. To the best of our knowledge, no studies are available in the literature which review and compare different constitutive models with the aim of establishing their capability to capture experimental data on human aortic valve. Hence, the intention of this work is to go a first step further in this direction.

Moving from the hypothesis of no cumbersome constitutive models, we refer to invariant–based constitutive models largely used in the literature to describe the nonlinear, incompressible anisotropic behavior of many soft tissues [28, 31, 33]. Then, it follows the objective of this study which is to compare the different constitutive models through a numerical optimization scheme and to collect properly material parameters that should be employed in computational tools to asses more realistic results. In fact, a drawback of most computational simulations is exactly the simplification of aortic sinuses material properties as being isotropic and linear elastic. The predictive ability of computational modeling is also compromised by the use of porcine experimental data which are very different from those of humans as evidenced histologically in recent studies [52, 53, 89].

Most of the investigated models basically provide a good fit of the experimental data as evidenced by the found NRMSE errors and the trend of the predicted stress-strain curves. For the experimental data of Martin et al. [52, 53],

Table 4 Calibrations of the identified SEFs with respect to the experimental data of Martin and Sun [53] (aortic valve leaflets)

Ψ	Sample	Material parameters				α	NRMSE
		c (kPa)	c_0 (kPa)	c_1 (–)	c_2 (–)		
Weinberg et al. [77]	LCL	14.87	8.26	170.0	$7.74{\cdot}10^{+7}$	–	0.2334
	NCL	16.44	2.85	534.4	$1.36{\cdot}10^{+7}$		0.0935
	RCL	2.34	5.68	130.6	$2.28{\cdot}10^{+5}$		0.0653
	mean	11.23	5.59	278.9	$3.04{\cdot}10^{+7}$	–	0.1307
	±SD	7.74	2.72	223.5	$4.12{\cdot}10^{+7}$		0.0900
Prot et al. [78]	LCL	34.69	0.43	1142.3	1607.9	–	0.2142
	NCL	33.06	0.56	1358.3	497.7		0.0523
	RCL	6.12	2.09	266.7	43.50		0.0364
	mean	24.62	1.03	922.4	716.4	–	0.1010
	±SD	16.05	0.92	578.1	804.8		0.0984
Humphrey et al. [28]	LCL	0.41	73.29	54.83	66.05	2	0.1994
	NCL	0.34	26.74	68.22	67.64		0.0856
	RCL	0.25	11.01	47.14	47.21		0.0352
	mean	0.33	37.02	56.73	60.30	2	0.1067
	±SD	0.08	32.38	10.67	11.36		0.0841
Humphrey—α	LCL	0.47	35.88	52.11	15.55	3	0.1898
	NCL	0.36	15.33	66.39	14.17		0.0766
	RCL	0.30	8.55	43.89	8.02		0.0254
	mean	0.38	19.92	54.13	12.58	3	0.0973
	±SD	0.08	14.23	11.39	4.01		0.0841

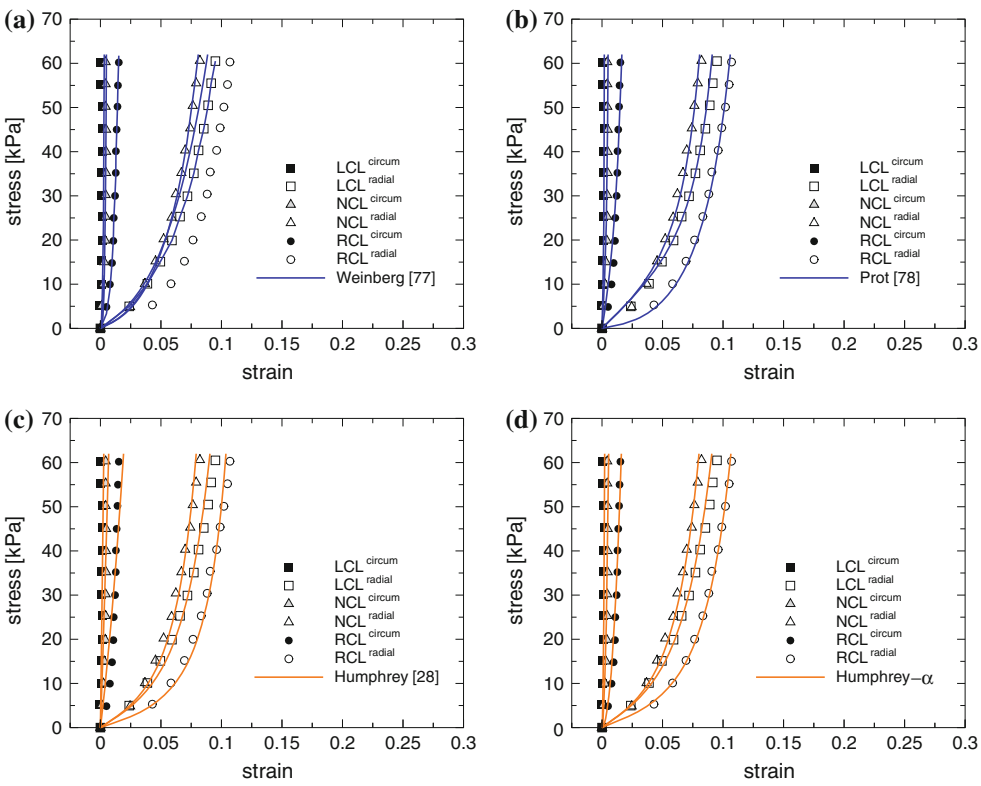

Fig. 4 Fitting results on the experimental data of Martin and Sun [53] (aortic valve leaflets) by using the SEFs of: Weinberg et al. [77]; Prot et al. [78]; Humphrey et al. [28] the proposed modified model with $\alpha = 3$

it is also possible to check the quality of our results referring to the mean value ± standard error provided by the authors.

However, a more detailed inspection points out that not all are able to capture well the data over the whole range of variability of the stresses in both the tensile directions and for each considered experimental study as, for example, the models of Weinberg and Kaazempur-Mofrad [77] and May-Newman and Yin [31] in the radial and circumferential directions for the aortic leaflets and the model of Holzapfel et al. [33] in the axial and radial directions for the aortic sinuses and aortic leaflets, respectively. On the contrary, the proposed Humphrey—α model has showed a very good ability to capture both the radial/axial and circumferential responses at low and higher stress values for aortic valve leaflets/sinuses.

It is worth noting that all of the optimizations performed on the uniaxial data of Stradins et al. [85] as well as the optimizations performed on the biaxial data of Martin and Sun [53] with only the Prot et al. [78] provide only one minimun, i.e. the global one. In the other cases, we find global minimum and more local minima. In some cases, this occurrence is due to the assumed values of TolX and TolFun (10^{-2}) whereby the solver see as distinct solutions very closed sets of material parameters.

However, some limitations affect our study. On one hand, with respect to the constitutive modeling, firstly, the contribution of each layer of the valvular tissues is disregarded assuming the material homogeneous through the thickness, as well as it is disregarded the angular fiber distribution. Secondly, the residual stresses which redistribute the stress field through the thickness are not considered in the constitutive equations.

To our knowledge, firstly, no tests have been performed on the dissected layers of human aortic valve, but only on porcine specimens [90]; our assumption, however, is motivated by the difficult to discern the spongiosa layer in human leaflets [53]. Secondly, experiments needed to assess residual strains in the aortic valve are not trivial to carry out due to the complex geometry of the aortic root system [45, 89].

At the same time also, with respect to the experimental data, the determination of the material constants relies on a very limited number of data set to make a consistent prediction for the mechanical behavior of aortic valve; we think this is mainly a literature limitation. In addition, in-vitro biaxial tests (and in particular uniaxial tests performed in only one direction) which require tissue excision are not suitable to capture the effective behavior of a structure with complex boundary conditions and physiological loads. In order to overcome this limitation, in vivo global measurements of the loading/deformation state could be necessary, and to make in vivo characterization tractable, a reliable inverse method could be needed. Actually, to the authors knowledge there are no useful references in this sense.

5 Conclusion

Even though our results are not general due to the paucity of experimental data on human aortic valve and to the material behavior assumptions, we have reviewed various models which may be adopted for modeling the aortic valve tissue behavior. The considered models have been fitted with respect to available data on human aortic valves and their predictions are assessed providing the opportunity of a critical comparison.

Acknowledgements The support of the Cariplo Foundation through the project number n.2009.2822 is gratefully acknowledged.

A stress components

A.1 Stresses in aortic leaflets

Aortic leaflet tissue is a material reinforced with a single class of fibers circularly oriented. We select a base vectors ($\mathbf{e}_1$, $\mathbf{e}_2$, $\mathbf{e}_3$) with the plane $\mathbf{e}_1$–$\mathbf{e}_2$ coincident with the plane of the specimen. The unit vector $\mathbf{e}_3$ is normal to the sheet plane. In the plane $\mathbf{e}_1$–$\mathbf{e}_2$, the unit vector $\mathbf{e}_1$ lies coaxial with the mean fiber direction $\mathbf{a}_0$ (i.e., the circumferential direction) while the unit vector $\mathbf{e}_2 = \mathbf{e}_3 \times \mathbf{e}_1$. We assume the one-fiber family embedded in the plane $\mathbf{e}_1$–$\mathbf{e}_2$, so that the fiber direction is $\mathbf{a}_0 \equiv \mathbf{e}_1$, in the reference configuration, and $\mathbf{a} = \mathbf{F}\mathbf{e}_1$, in the current configuration.

In terms of the principal stretches, λ_1, λ_2, λ_3, which satisfy the incompressibility constraint $\lambda_3 = (\lambda_1\lambda_2)^{-1}$, the invariants I_1 and I_4 are given by:

$$I_1 = \lambda_1^2 + \lambda_2^2 + (\lambda_1\lambda_2)^{-2}, \qquad I_4 = \lambda_1^2. \tag{13}$$

The non-zero components of the Cauchy stress tensor, σ_{11} and σ_{22}, are given by:

$$\begin{aligned} \sigma_{11} &= 2\Psi_1\left[\lambda_1^2 - (\lambda_1\lambda_2)^{-2}\right] + 2\Psi_4\lambda_1^2, \\ \sigma_{22} &= 2\Psi_1\left[\lambda_2^2 - (\lambda_1\lambda_2)^{-2}\right]. \end{aligned} \tag{14}$$

Noting that the Lagrange multiplier $p = 2\Psi_1(\lambda_1\lambda_2)^{-2}$ has been determined from the plain stress condition $\sigma_3 = 0$.

In the particular case of uniaxial tensile test, the stress $\sigma_{22} = 0$, then, it follows from Eq. $(14)_2$ that $\lambda_2 = \lambda_1^{-1/2}$ and from Eq. $(14)_1$ that the only one non-zero stress component is $\sigma_{11} = 2\Psi_1\left[\lambda_1^2 - \lambda_1^{-1}\right] + 2\Psi_4\lambda_1^2$.

A.2 Stresses in aortic sinuses

Aortic sinuses tissue is a material reinforced with two class of fibers symmetrically oriented with respect to the circumferential direction at angles $\pm\vartheta$ in the reference configuration.

We select a base vectors ($\mathbf{e}_1$, $\mathbf{e}_2$, $\mathbf{e}_3$) so that the $\mathbf{e}_1$–$\mathbf{e}_2$ plane coincides with the sheet plane where the fibers are embedded and the unit vector $\mathbf{e}_3$ is normal to this plane. Hence, in the reference configuration, the fiber directions are: $\mathbf{a}_0 = \cos\vartheta\mathbf{e}_1 + \sin\vartheta\mathbf{e}_2$ and $\mathbf{b}_0 = \cos\vartheta\mathbf{e}_1 - \sin\vartheta\mathbf{e}_2$, whereas their spatial counterparts become: $\mathbf{a} = \lambda_1\cos\vartheta\mathbf{e}_1 + \lambda_2\sin\vartheta\mathbf{e}_2$ and $\mathbf{b} = \lambda_1\cos\vartheta\mathbf{e}_1 - \lambda_2\sin\vartheta\mathbf{e}_2$, respectively.

In terms of the principal stretches, λ_1, λ_2, $\lambda_3 = (\lambda_1\lambda_2)^{-1}$, the invariants I_1 I_4 and I_6 are given by:

$$I_1 = \lambda_1^2 + \lambda_2^2 + (\lambda_1\lambda_2)^{-2},$$
$$I_4 = I_6 = \lambda_1^2\cos^2\vartheta + \lambda_2^2\sin^2\vartheta. \quad (15)$$

Assuming that the to fiber classes are mechanically equivalent such that $\Psi_1 = \Psi_2$, the non-zero components of the Cauchy stress tensor, σ_{11} and σ_{22}, are given by:

$$\sigma_{11} = 2\Psi_1\left[\lambda_1^2 - (\lambda_1\lambda_2)^{-2}\right] + 2\Psi_4\lambda_1^2\cos^2\vartheta,$$
$$\sigma_{22} = 2\Psi_1\left[\lambda_2^2 - (\lambda_1\lambda_2)^{-2}\right] + 2\Psi_4\lambda_1^2\sin^2\vartheta. \quad (16)$$

References

1. Yacoub MH, Takkenberg JJ (2005) Will heart valve tissue engineering change the world? Nat Clin Pract Cardiovasc Med 2:60–61
2. Nkomo VT, Gardin JM, Skelton TN, Gottdiener JS, Scott CG, Enriquez-Sarano M (2006) Burden of valvular heart diseases:a population-based study. Lancet 368:1005–1011
3. Otto CM (2006) Valvular aortic stenosis: diseases severity and timing of intervention. J Am Coll Cardiol 47:2141–2151
4. Filová E, Straka F, Miřejovský T, Mašín J, Bačáková L (2009) Tissue-engineered heart valves. Physiol Res 58 (Suppl 2):S141–S158
5. Grande KJ, Cochran RP, Reinhall PG, Kunzelman KS (2000) Recreation of sinuses is important for sparing the aortic valve: a finite element study. J Thorac Cardiovasc Surg 119:753–763
6. Gnyaneshwar R, Kumar KR, Balakrishnan RK (2002) Dynamic analysis of the aortic valve using a finite element model. Ann Thorac Surg 73:1122–1129
7. Soncini M, Votta E, Zinicchino S, Burrone V, Mangini A, Lemma M, Antona A, Redaelli C (2009) Aortic root performance after valve sparing procedure: a comparative finite element analysis. Med Eng Phys 31:234–243
8. Auricchio F, Conti M, Morganti S (2011) Finite element analysis of aortic root dilation: a new procedure to reproduce pathology based on experimental data. Comput Methods Biomech Biomed Eng
9. Gupta BS, Kasyanov VA (1997) Biomechanics of human common carotid artery and design of novel hybrid textile compliant vascular grafts. J Biomed Mater Res 34:341–349
10. Demiray H (1972) A note on the elasticity of soft biological tissues. J Biomech 5:309–311
11. Fung YC, Fronek K, Patitucci P (1979) Pseudoelasticity of arteries and the choice of its mathematical expression. Am J Physiol 237:H620–H631
12. Chuong CJ, Fung YC (1983) Three-dimensional stress distribution in arteries. J Biomech Eng 105:268–274
13. Takamizawa K, Hayashi K (1987) Strain energy density function and uniform strain hypotesis for arterial mechanics. Biophys J 20:7–17
14. Weinberg EJ, Shahmirzadi D, Mofrad MR (2010) On the multiscale modeling of heart valve biomechanics in health and disease. Biomech Model Mechanobiol 9:373–387
15. Holzapfel GA, Stadler TC, Gasser M. (2002) A structural model for the viscoelastic behavior of arterial walls: continuum formulation and finite element analysis. Eur J Mech A Solids 21:441–463
16. Rowe AJ, Finlay HM, Canham PB (2003) Collagen biomechanics in cerebral arteries and bifurcations assessed by polarizing microscopy. J Vasc Res 40:406415
17. Cacho F, Elbischger PJ, Rodrguez JF, Doblar M, Holzapfel GA (2007) A constitutive model for fibrous tissues considering collagen fiber crimp. Int J Non Linear Mech 42:391-402
18. Tang D, Teng Z, Canton G, Yang C, Ferguson M, Huang X, Zheng J, Woodard PK, Yuan C (2009) Sites of rupture in human atherosclerotic carotid plaques are associated with high structural stresses. An in vivo mri-based 3d fluid-structure interaction study. Stroke 40:3258–3263
19. Maceri F, Marino M, Vairo G (2010) A unified multiscale mechanical model for soft collagenous tissues with regular fiber arrangement. J Biomech 43:355-363
20. Humphrey JD (2003) Continuum biomechanics of soft biological tissues. R Soc 459:3–46
21. Spencer AJM (1982) Deformation of fiber-reinforced materials. Oxford University Press, Oxford
22. Spencer AJM (1984) Continuum theory of the mechanics of fibre-reinforced composites. Springer, New York
23. Lanir Y (1983) Constitutive equations for fibrous connective tissues. J Biomech 16:1–12
24. Gasser TC, Ogden RW, Holzapfel GA (2006) Hyperelastic modelling of arterial layers with distributed collagen fibre orientations. J R Soc Interf 3:15–35
25. Billiar KL, Sacks MS (2000) Biaxial mechanical properties of the natural and glutaraldehyde treated aortic valve cusp—part I: experimental results. J Bioeng 122:23–30
26. Sacks MS, Sun W (2003) Multiaxial mechanical behavior of biological materials. Ann Rev Biomed Eng 5:251–284
27. Driessen NJB, Bouten CVC, Baaijens FPT (2005) Improved prediction of the collagen fiber architecture in the aortic heart valve. J Bioeng 127:329–336
28. Humphrey JD, Yin FCP (1987) On constitutive relations and finite deformations of passive cardiac tissue: I. A pseudostrain–energy function. J Biomech Eng 109:298–304
29. Humphrey JD, Yin FCP (1989) Biomechanical experiments on excised myocardium: Theoretical considerations. J Biomech 22:377–383
30. May-Newman K, Yin FCP (1995) Biaxial mechanical behavior of excised porcine mitral valve leaflets. Am Physiol Soc 269:H1319–H1327
31. May-Newman K, Yin FCP (1998) A constitutive law for mitral valve tissue. J Bioeng 120:38–47
32. Hayashi K (1993) Experimental approaches on measuring the mechanical properties and constitutive laws of arterial walls. J Biomech Eng 115:481-488

33. Holzapfel GA, Gasser TC, Ogden RW (2000) A new constitutive framework for arterial wall mechanics and a comparative study of material models. J Elast 61:1–48
34. Grande KJ, Cochran RP, Reinhall PG, Kunzelman KS (2000) Mechanisms of aortic valve incompetence: finite element modeling of aortic root dilatation. Ann Thorac Surg 69:1851–1857
35. Grande KJ, Cochran RP, Reinhall PG, Kunzelman KS (2001) Mechanisms of aortic valve incompetence: finite-element modeling of marfan syndrome. J Thorac Cardiovas Surg 122:946–954
36. Grande KJ, Cochran RP, Reinhall PG, Kunzelman KS (1998) Stress variations in the human aortic root and valve: the role of anatomic asymmetry. Ann Biomed Eng 26:534–545
37. Beck A, Thubrikar MJ, Robicsek F (2001) Stress analysis of the aortic valve with and without the sinuses of valsalva. JHVD 10:1–11
38. Katayama S, Umetani N, Sugiura S, Hisada T (2008) The sinus of valsalva relieves abnormal stress on aortic valve leaflets by facilitating smooth closure. J Heart Valve Dis 136:1528–1535
39. Missirlis YF, Chong M. (1978) Aortic valve mechanics—part i: material properties of natural porcine aortic valves. J Bioeng 2:287–300
40. Sauren AAHJ, van Houta MC, van Steenhovena AA, Veldpausa FE, Janssena JD (1983) The mechanical properties of porcine aortic valve tissues. J Biomech 16:327–337
41. May-Newman K, Lam C, Yin FCP (2009) A hyperelastic constitutive law for aortic valve tissue. J Bioeng 131:1–7
42. Adamczyk MM, Vesely I (2002) Characteristics of compressive strains in porcine aortic valves cusps. J Heart Valve Dis 11:75–83
43. Merryman WD, Engelmayr GC, Liao J, Sacks MS (2006) Defining biomechanical endpoints for tissue engineered heart valve leaflets from native leaflet properties. Prog Pediatr Cardiol 21:153–160
44. Sauren AAHJ, Kuijpers W, van Steenhovena AA, Veldpaus FE (1980) Aortic valve histology and its relation with mechanics –preliminary report. J Biomech 13:97–104
45. Gundiah N, Kam K, Matthews PB, Guccione J, Dwyer HA, Saloner D, Chuter TAM, Guy TS, Ratcliffe MB, Tseng EE (2008) Asymmetric mechanical properties of porcine aortic sinuses. Ann Thorac Surg 85:1631–1638
46. Matthews PB, Azadani AN, Jhun C, Ge L, Guy TS, Guccione JM, Tseng EE (2010) Comparison of porcine pulmonary and aortic root material properties. Ann Thorac Surg 89:1981–1989
47. Sands MP, Rittenhouse EA, Mohri H, Merendino KA (1969) An anatomical comparison of human, pig, calf and sheep aortic valves. Ann Thorac Surg 8:407–414
48. Balasundari R, Gupta R, Sivasubramanian V, Chandrasekaran R, Arumugam S, Cherian KM, Guhathakurta S. (2007) Complete microbe free processed porcine xenograft for clinical use. Indian J Thorac Cardiovasc Surg 23:240–245
49. Nicosia MA, Kasalko JS, Cochran RP, Einstein DR, Kunzelman KS (2002) Biaxial mechanical properties of porcine ascending aortic wall tissue. J Heart Valve Dis 11:680–687
50. Sim EKW, Muskawad S, Lim S, Yeo JH, Lim KH, Grignani RT, Durrani G, Lau A, Duran C (2003) Comparison of human and porcine aortic valves. Clin Anat 16:193–196
51. Martin T, Pham C, Sun W (2010) Difference in mechanical properties between human and porcine aortic root. In: Proceedings of the annual international conference of the IEEE
52. Martin C, Pham T, Sun W (2011) Significant differences in the material properties between aged human and porcine aortic tissues. Eur J Cardiothorac Surg 40:28–34
53. Martin C, Sun W (2012) Biomechanical characterization of aortic valve tissue in humans and common animal models. J Biomed Mater Res Part A 100A:1591–1599
54. Hokken RB, Bartelings MM, Bogers AJ, Gittenberger-DeGroot AC (1997) Morphology of the pulmonary and aortic roots with regard to the pulmonary autograft procedure. J Thorac Cardiovasc Surg 113:453–461
55. Sacks MS, Smith MS, Hiester ED (1998) The aortic valve microstructure: Effect of transvalvular pressure. J Biomed Mater Res 41:131–141
56. Misfeld M, Sievers H (2007) Heart valve macro- and microstructure. Philos Trans R Soc B 362:1421–1436
57. Taylor PM (2007) Biological matrices and bionanotechnology. Philos Trans R Soc B 362:1313–1320
58. Sacks MS, Merryman WD, Schmidt DE (2009) On the biomechanics of heart valve function. J Biomech 42:1804–1824
59. Gambarin FI, Massetti M, Dore R, Saloux E, Favalli V, Arbustini V (2010) The aortic root. In: Saremi F, Achenbach S, Arbustini E, Narula J (eds). Revisiting cardiac anatomy: a computed-tomography-based Atlas and reference. Wiley-Blackwell, Oxford
60. Hinton RB, Yutzey KE (2011) Heart valve structure and function in development and disease. Ann Rev Physiol 73:41–418
61. Bashey RI, Torii S, Angrist A (1967) Age-related collagen and elastin content of human heart valves. J Gerontol 22:203–208
62. Ferrans VJ, Hilbert SL, Tomita T, Jones M, Robert WC (1988) Morphology of collagen in bioprosthetic heart valves. In: Nimni ME, Boca Raton FL (eds) Collagen 3. CRC Press, pp 145–189
63. Scott MJ, Vesely I (1996) Morphology of porcine aortic valve cusp elastin. J Heart Valve Dis 5:464–471
64. Schriefl AJ, Regitnig P, Pierce DM, Holzapfel GH (2011) Layer-specific distributed collagen fiber orientations in human arteries, from thoracic aorta to common iliac. In: Proceedings of the ASME 2011 summer bioengineering conference, Farmington, Pennsylvania, USA, June 22–25, pp 1–2
65. Clark RE, Butterworth GAM (1971) Characterization of the mechanics of human aortic and mitral valve leaflets. Surg Forum 22:134–136
66. Swanson WM, Clark RE (1974) Dimensions and geometric relationships of the human aortic valve as a function of pressure. Circ Res 22:871–882
67. Bairati A, De Biasi S (1981) Presence of a smooth muscle system in aortic valve leaflets. Anat Embryol (Berl) 161:329–340
68. Vesely I, Noseworthy R (1992) Micromechanics of the fibrosa and the ventircularis in aortic valve leaflets. J Biomech 25:101–113
69. Sacks MS, Smith DB, Hiester ED (1997) A small angle light scattering device for planar connective tissue microstructural analysis. Ann Biomed Eng 25:678–689
70. Weiss JA, Maker BN, Govindjee S (1996) Finite element implementation of incompressible, transversely isotropic hyperelasticity. Comput Methods Appl Mech Eng 135:107–128
71. Merodio J, Ogden RW (2003) Instabilities and loss of ellipticity in fiber-reinforced compressible non-linearly elastic solids under plane deformation. Int J Solids Struct 40:4707–4727
72. Merodio J, Ogden RW (2005) On tensile instabilities and ellipticity loss in fiber-reinforced incompressible non-linearly elastic solids. Mech Res Commun 32:290–299
73. Merodio J, Ogden RW (2006) The influence of the invariant i8 on the stress-deformation and ellipticity characteristics of doubly fiber-reinforced non-linearly elastic solids. Int J Non-linear Mech 41:556–563
74. Holzapfel GA, Ogden RW (2009) On planar biaxial tests for anisotropic nonlinearly elastic solids a continuum mechanical framework. Math Mech Solids 14:474–489
75. Humphrey JD, Strumpf RK, Yin FCP (1990) Determination of a constitutive relation for passive myocardium: I. a new functional form. J Biomech Eng 112:333–339
76. Prot V, Skallerud B, Holzapfel GA (2007) Transversely isotropic membrane shells with application to mitral valve mechanics. constitutive modelling and finite element implementation. Int J Numer Methods Eng 71:987–1008

77. Weinberg EJ, Kaazempur-Mofrad MR (2006) A large-strain finite element formulation for biological tissues with application to mitral valve leaflet tissue mechanics. J Biomech 39: 1557–1561
78. Prot V, Skallerud B, Sommer G, Holzapfel GA (2010) On modelling and analysis of healthy and pathological human mitral valves: two case studies. J Mech Behav Biomed Mater 3:167–177
79. Holzapfel GA, Weizsäcker HW (1998) Biomechanical behavior of the arterial wall and its numerical characterization. Comput Biol Med 28(4):377–392
80. Stålhand J, Klarbring A, Karlsson M (2004) Towards in vivo aorta material identification and stress estimation. Biomech Model Mechanobiol 2:169–186
81. Holzapfel GA, Sommer G, Gasser CT, Regitnig P (2005) Determination of layer-specific mechanical properties of human coronary arteries with nonatherosclerotic intimal thickening and related constitutive modeling. Am J Physiol Heart Circ Physiol 289:H2048–H2058
82. Stålhand J (2009) Determination of human arterial wall parameters from clinical data. Biomech Model Mechanobiol 8:141–148
83. Konig K, Schenke-Layland K, Riemann I, Stock UA (2005) Multiphoton autofluorescence imaging of intratissue elastic fibers. Biorheology 26:495–500
84. Schenke-Layland K, Riemann I, Stock UA, Konig K (2005) Morphology of porcine aortic valve cusp elastin. J Biomed Opt 10:024017
85. Stradins P, Lacis I, Ozolanta R, Burina B, Ose V, Feldmane L, Kasyanov V (2004) Comparison of biomechanical and structural properties between human aortic and pulmonary valve. Eur J Cardiothoracic Surg 26:634–639
86. Milnor WR (1989) Hemodynamics. Williams & Wilkins, Baltimore
87. Sacks MS (1999) A method for planar biaxial mechanical testing that includes in-plane shear. J Bioeng 121:551–555
88. Holzapfel GA, Sommer G (2004) Anisotropic mechanical properties of tissue components in human atherosclerotic plaques. J Biomech Eng 126:657–665
89. Azadani AN, Chitsaz S, Matthews PB, Jaussaud N, Leung T, Tsinman J, Ge V, Tseng EE (2012) Comparison of mechanical properties of human ascending aorta and aortic sinuses. Ann Thorac Surg 93:87–94
90. Stella JA, Sacks MS (2007) On the biaxial mechanical properties of the layers of the aortic valve leaflet. J Bioeng 129:757–766